

A Stable Transition Controller for Constrained Robots

Prabhakar R. Pagilla, *Member, IEEE*, and Biao Yu

Abstract—This paper addresses the problem of contact transition from free motion to constrained motion for robots. Stability of transition from free motion to constrained motion is essential for successful operation of a robot performing general tasks such as surface following and surface finishing. Uncertainty in the location of the constraint can cause the robot to impact the constraint surface with a nonzero velocity, which may lead to bouncing of the robot end-effector on the surface. A new stable discontinuous transition controller is proposed to deal with contact transition problem. This discontinuous transition control algorithm is used when switching from free motion to constrained motion. Control algorithm for a complete robot task is developed. Extensive experiments with the proposed control strategy were conducted with different levels of constraint uncertainty and impact velocities. Experimental results show much improved transition performance and force regulation with the proposed controller. Details of the experimental platform and typical experimental results are given.

Index Terms—Discontinuous control, force control, impact, Lyapunov stability, robot control, unilateral constraint.

I. INTRODUCTION

THE contact transition control problem from free motion to constrained motion for geometrically constrained robots is the main focus of this paper. Many industrial applications of robots involve interaction between the robot and an environment, which is generally a workpiece or an external object. Robotic surface finishing is one such application where the robot makes and breaks contact with the workpiece in the process of surface finishing. For such applications, the complete task of the robot typically involves motion in its workspace before making contact with the surface. After stable contact with the surface, the goal is to follow the surface while performing the required surface finishing task, which is the constrained motion phase. This requires trajectory tracking tangential to the constraint surface while regulating a desired force normal to the surface.

Switching from free motion to constrained motion of the robot leads to stability problems, which is reported extensively in the robotics literature. The contact transition problem is of more severe nature if the robot makes contact with the surface with a nonzero velocity normal to the constraint surface. In this case, the robot experiences large impact forces and the end-effector has a tendency to bounce on the surface. The severity of these bounces mostly depend on the magnitude

of the impact velocity and the rigidity of the surface and end-effector assembly. Switching directly from free motion control to simultaneous motion and force control upon making contact with the surface leads to stability problems. Since a large impact force is experienced at impact, force feedback just after contact with the surface may aggravate the tendency of the end-effector to bounce on the surface. It is necessary to regulate the velocity normal to the constraint surface to zero before simultaneous motion and force control strategy is used. Hence, the primary control goal during transition from free motion to constrained motion is to regulate the velocity normal to the surface to zero after the end-effector makes contact with the constraint surface.

Extensive research has been done in free motion control of robots and constrained motion and force control assuming that the robot is on the surface. A large body of research in free motion control and constrained motion and force control has been reported in [1] and [2] and the references therein. Most of the research in constrained motion and force control has been based on the assumption that the robot is already in contact with the constraint surface [3]–[7].

Early work on mathematical modeling of a robot colliding with a surface can be found in [8]. The external environment is treated as a mechanical impedance, and impedance control is used in contact transition experiments in [9] and [10]. Stability and control of task transition for robots for a compliant environment are considered in [12]. Force regulation and contact transition control using positive acceleration feedback together with a switching control strategy were developed in [15]. A contact transition control algorithm for nonlinear mechanical systems subject to a unilateral constraint was developed in [14]. A dimensionless representation of impact behavior was developed in [16]. The contact problem for linear continuous-time dynamical systems with inequality constraints is considered in [17]. A definition of contact and release sets from a system theoretic framework is considered in this paper. Control of finite-dimensional mechanical systems with unilateral constraints is discussed in [18]. The closed-loop control problem for such systems is analyzed with various switching control strategies. Control laws for the regulation problem of mechanical systems with inequality constraints are proposed in [19]. Formulation of mechanical systems with geometric inequality constraints as complementarity systems can be found in [27].

Since the contact problem involves collision of the robot with a surface, knowledge of the impact phenomena is required to describe the behavior of the robot after impact with the surface. Impact models are necessary for determining the post-impact velocities based on aspects such as the impact phenomena, pre-impact velocity, stiffness and compliance of the surface, and configuration of the system at impact. Extensive research in the

Manuscript received January 26, 2000. Recommended by Technical Editor R. Isermann. This work was supported in part by the National Science Foundation under Grant CMS-9700026.

The authors are with the School of Mechanical and Aerospace Engineering, Oklahoma State University, Stillwater, OK 74078-5016 USA (e-mail: pagilla@okstate.edu; ybiao@okstate.edu).

Publisher Item Identifier S 1083-4435(01)02725-9.

area of impact behavior and modeling can be found in the mechanics literature [20]–[22]. Recent results and an extensive bibliography in nonsmooth impact mechanics can be found in [23].

Most of the contact transition algorithms that have been proposed assume that the environment is compliant and/or an impact model exists for the surface that can be used in the control algorithm. Further, most control algorithms dealing with the contact transition problem are analytical results and have not been experimentally verified for a complete task. In this paper, we design a new stable contact transition controller for contact transition from free motion to constrained motion. The transition control algorithm does not require explicit knowledge of the impact model. But existence of an impact model is assumed for stability analysis. Most of the studies in contact transition problem are based on transformation of the joint space coordinates to a set of coordinates that represent normal and tangential directions of the surface. This is not convenient from an implementation perspective, as controllers are designed based on the transformed coordinates. Moreover, the control algorithm designed in the transformed coordinates can cause implementation problems if the constraint surface location is not known exactly. In this paper, we use the orthogonalization principle and the projection matrices given in [1]. The basic control algorithm on which we build the proposed control algorithm for a complete task is the model-based control algorithm given in [1] and [2].

Extensive robotic surface following experiments were conducted using the proposed control design methodology. The constraint surface is assumed to be frictionless. Uncertainty in the location of the constraint is considered as the main cause for impact of the robot with the constraint surface. Different levels of constraint uncertainty and travel speeds of the robot end-effector are considered in the experiments. It is shown that the performance of the proposed control strategy with a new transition controller is much improved when compared with directly switching from free motion to constrained motion and force control.

The rest of this paper is organized as follows. In Section II, a dynamic model for constrained robots that can be used in control design is developed. Impact models and their use in contact transition problem is also discussed in Section II. A control design for a complete task that includes free motion, transition phase, and constrained motion is given in Section III. Experimental platform and experimental results are given in Section IV. Conclusions and future research are given in Section V.

II. DYNAMIC MODEL FOR CONSTRAINED ROBOTS

Let the kinetic and potential energy functions of the n -link robot be given by $\mathcal{K}(q, \dot{q}) = (1/2)\dot{q}^T M(q)\dot{q}$ and $\mathcal{P}(q)$, where $q, \dot{q} \in \mathbb{R}^n$ are the generalized position and velocity, respectively, and $M(q) \in \mathbb{R}^{n \times n}$ is the symmetric positive definite mass matrix. Let the geometric constraint on the robot be modeled by the following unilateral constraint [14]:

$$\phi(x(q)) - d \leq 0 \quad (1)$$

where $x(q)$ is the Cartesian position and d is a constant that gives the location of the constraint surface. It is assumed that the constraint uncertainty is due to its location, i.e., in (1), $\phi(x(q))$ is

exactly known but d may not be accurately known. Define the following orthogonal projection matrix [7] whose image represents the normal direction of the constraint:

$$P_\phi(q) = [\nabla\phi(x(q))][\nabla\phi(x(q))]^T / \|\nabla\phi(x(q))\|^2$$

and the kernel of $P_\phi(q)$ gives the tangential direction of the constraint and is given by

$$Q_\phi(q) = I_n - P_\phi(q)$$

where I_n denotes the $n \times n$ identity matrix. Notice that both the normal and tangential projection matrices depend on $\phi(x(q))$, and hence they are exactly known. The dynamics of the geometrically constrained robot is

$$M(q)\ddot{q} + C(q, \dot{q})\dot{q} + g(q) = \tau + v(q)f_n \quad (2)$$

where $C(q, \dot{q}) \in \mathbb{R}^{n \times n}$ is the matrix composed of Coriolis and centripetal terms; $g(q) \in \mathbb{R}^n$ is the gravity vector; $\tau \in \mathbb{R}^n$ is the generalized force applied by the motors at each joint of the robot; $f_n \in \mathbb{R}$ is the magnitude of the normal contact force; and $v(q) \in \mathbb{R}^n$ maps the normal force magnitude into corresponding joint forces, and is given by

$$v(q) = J^T(q)n(x(q))$$

where $n(x(q)) = \nabla\phi(x(q))/\|\nabla\phi(x(q))\|$ is the unit surface normal vector in Cartesian coordinates and $J(q)$ is the Jacobian of the manipulator. Notice that the dynamics given by (2) does not contain the tangential component of the contact force because the surface is assumed to be frictionless. The magnitude of the normal force f_n depends on the activation/deactivation of the constraint. That is, if $\phi(q) < 0$, then $f_n = 0$, and if $\phi(q) = 0$, then $f_n \geq 0$.

A complete task of the robot in the presence of the unilateral constraint can be divided into the following three phases:

- 1) when $\phi(q) < 0$, then $f_n = 0$, and the robot is said to be in the free motion phase;
- 2) when $\phi(q) = 0$ and $f_n > 0$, then the robot is said to be in the constrained motion phase;
- 3) transition from the free motion phase to the constrained motion phase is termed as the transition phase.

The presence of the unilateral constraint in the robot workspace divides the state space into the following sets:

$$X_c := \{q, \dot{q} \in \mathbb{R}^n : \phi(q) = 0\} \quad (3)$$

$$X_u := \{q, \dot{q} \in \mathbb{R}^n : \phi(q) < 0\} \quad (4)$$

$$X_f := \{q, \dot{q} \in \mathbb{R}^n : \phi(q) > 0\} \quad (5)$$

where

X_c state space when the robot lies on the constraint surface;

X_u state space in which the robot can freely move;

X_f state space that violates the constraint.

The space X_c can be further subdivided into sets X_{ct} and X_{ca} , i.e., $X_c = X_{ct} \cup X_{ca}$, given by

$$X_{ct} := \{q, \dot{q} \in \mathbb{R}^n : \phi(q) = 0, P_\phi(q)\dot{q} \neq 0\} \quad (6)$$

$$X_{ca} := \{q, \dot{q} \in \mathbb{R}^n : \phi(q) = 0, P_\phi(q)\dot{q} = 0\} \quad (7)$$

where $P_\phi(q)\dot{q}$ indicates joint velocity component that is normal to the constraint surface. The motivation for this subdivision is that the system can impact the constraint surface with a nonzero normal velocity, and there is a jump condition in velocity. The post-impact velocity of the robot is generally determined based on an impact model and pre-impact velocity. Depending on the velocity of impact and the rigidity of the constraint surface, the robot end-effector may bounce on the surface. The transition phase starts when the the robot makes the first impact with the surface and lasts until stable contact is made with the surface with zero normal velocity. With the subdivision of the state space, the dynamics in each phase can be written as follows.

If $q, \dot{q} \in X_u$, then the dynamic equations are

$$M(q)\ddot{q} + C(q, \dot{q})\dot{q} + g(q) = \tau. \quad (8)$$

If $q, \dot{q} \in X_{ct}$, then the jump condition for (8) is given by

$$\dot{q}_+ = \mathcal{D}(q, \dot{q}_-). \quad (9)$$

\dot{q}_+ and \dot{q}_- represent the post- and pre-impact velocities, respectively, and $\mathcal{D}(\cdot)$ represents an operator that maps pre-impact velocity into post-impact velocity. This operator can take several forms depending on the choice of the impact model for the constraint surface. When the robot configuration lies in X_{ct} , then the jump discontinuity for the differential equation (8) is given by (9).

If $q \in X_{ca}$, then the dynamic equations are

$$M(q)\ddot{q} + C(q, \dot{q})\dot{q} + g(q) = \tau + v(q)f_n. \quad (10)$$

A. Impact Models

Impacts are generally treated as very large forces acting over a short duration of time. If we assume that the impact occurs over an infinitesimally small period of time, then 1) all velocities remain finite and 2) there is no change in position of the system. If Δt is the duration of collision and $F(\omega)$ is impact force during collision, then the force impulse F_I due to the impact at time t_* is given by

$$F_I = \lim_{\Delta t \rightarrow 0} \int_{t_*}^{t_* + \Delta t} F(\omega) d\omega. \quad (11)$$

At impact points, the dynamics become

$$M(q)\Delta\dot{q}(t_*) = F_I \quad (12)$$

where $\Delta\dot{q}(t_*) = \dot{q}(t_*^+) - \dot{q}(t_*^-)$. Since the surface is assumed to be frictionless, the force impulse F_I lies in the direction that is normal to the surface, i.e.,

$$Q_\phi F_I = 0 \quad \text{and} \quad P_\phi F_I = F_I. \quad (13)$$

We make two assumptions on the impact model: 1) there is kinetic energy reduction at every impact and 2) the impact map given by (9) has a dead zone with respect to the pre-impact and post-impact velocities, i.e., when the impact velocity becomes very small the robot end-effector sticks to the surface. The first assumption about kinetic energy reduction at impact is given by

$$\mathcal{K}^+ - \mathcal{K}^- = -\Delta\mathcal{K} < 0 \quad (14)$$

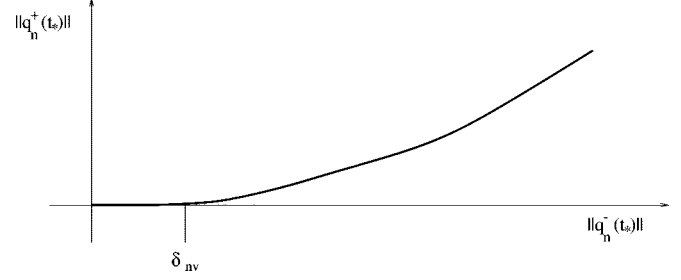


Fig. 1. Post-impact normal velocity versus pre-impact normal velocity.

where $\mathcal{K}^- = (1/2)(\dot{q}^-)^T M(q)(\dot{q}^-)$ and $\mathcal{K}^+ = (1/2)(\dot{q}^+)^T \cdot M(q)(\dot{q}^+)$ denote the pre-impact and post-impact kinetic energy, respectively, and $\Delta\mathcal{K}$ is a positive quantity. The second assumption can be illustrated as shown in Fig. 1, where $\dot{q}_{nt_*} := P_\phi \dot{q}_{t_*}$ denotes the joint velocity component normal to the surface. From Fig. 1, the post-impact velocity is zero when the pre-impact velocity is below a certain value, which is denoted by δ_{nv} .

III. CONTROL DESIGN FOR A COMPLETE TASK

The control goal is to track a desired trajectory, a part of which lies on the constraint surface. A typical complete task that is reflected in the desired trajectory is as follows: approach the surface, make contact with the surface, follow the surface while regulating the desired normal force, leave the surface, and return to the starting point. Therefore, the control objective in free motion phase is to track the desired motion trajectory. During constrained motion phase, the control objective is to simultaneously track the desired motion in the tangential direction and regulate the desired force in the normal direction of the constraint surface. Switching directly from free motion to simultaneous motion and force control in the constrained motion phase could lead to severe repeated impacts of the robot end-effector on the surface if there is an uncertainty in the constraint location. A transition control algorithm is required to stabilize the robot end-effector onto the surface. Therefore, in the transition phase, the control objective is to regulate the velocity normal to the surface to zero. In the following, we design a stable control algorithm for each phase.

A. Model-Based Control During Free Motion Phase

During this phase, the robot is away from the constraint surface and is in free motion. A number of control designs exist in literature that have been shown to work quite well for trajectory tracking. In this paper, an experimentally well tested passivity-type model-based controller is chosen for this phase. If the robot inertial parameters are not known exactly, then a model-based adaptive controller can be considered for this phase. We briefly give such a controller and its closed-loop error dynamics in this section. The model-based adaptive control law and parameter estimation laws are

$$\tau = Y(q, \dot{q}, \ddot{q}_r, \ddot{q}_r)\hat{\beta}(t) - F_v e_v \quad (15)$$

$$\hat{\beta}(t) = \beta_0 - \int_0^t \Gamma^{-T} Y^T(q, \dot{q}, \dot{q}_r, \ddot{q}_r) e_v(\omega) d\omega \quad (16)$$

where F_v, Γ are positive definite gain matrices, $\hat{\beta}(t)$ and β_0 are the estimate and initial known value of β , respectively, and

$$\begin{aligned} \dot{q}_r &= \dot{q}_d - \Lambda_p e \\ e_v &= \dot{q} - \dot{q}_r \\ Y(q, \dot{q}, \ddot{q}_r, \ddot{q}_r) \hat{\beta}(t) &= \hat{M}(q) \ddot{q}_r + \hat{C}(q, \dot{q}) \dot{q}_r + \hat{g}(q) \end{aligned}$$

where Λ_p is a positive definite gain matrix. Substituting the control law (15) into the robot dynamics (8) and rearranging terms results in the following error dynamics

$$M(q) \dot{e}_v + C(q, \dot{q}) e_v + F_v e_v = Y(q, \dot{q}, \ddot{q}_r, \ddot{q}_r) \tilde{\beta}(t) \quad (17)$$

where $\tilde{\beta}(t) = \hat{\beta}(t) - \beta$ is the parameter estimation error. Stability of the closed-loop system can be shown using standard Lyapunov techniques.

B. Discontinuous Control During Transition Phase

The transition phase starts when the robot makes its first impact with the surface and lasts until the robot makes a stable contact with the surface. The first impact gives the actual location of the constraint surface. The desired motion trajectory of the robot is developed based on *a priori* knowledge of the location of the constraint. The desired trajectory should be modified based on the actual location of the constraint, which is given by the first impact. After the first impact, the desired trajectory is modified using the projection matrices. The modified trajectory represents motion of the end-effector along the tangential direction of the constraint and regulation in the normal direction to the actual location of the constraint. Now, the control goal becomes regulation of the end-effector onto the surface and tracking of the modified desired trajectory in the tangential direction. Notice that the projection matrices do not depend on the uncertainty in the location of the constraint, which is the uncertainty in the constant d given in (1). From now on, we assume without loss of generality that the robot inertial parameters are known. The controller for the transition phase is chosen to be

$$\tau = Y(q, \dot{q}, \ddot{q}_r, \ddot{q}_r) \beta - F_v e_v - \lambda_{tn} P_\phi \text{sgn}(e_{vn}) \quad (18)$$

where $\text{sgn}(e_{vn})$ represents the component-wise sign of the vector e_{vn} , and

$$\begin{aligned} \dot{q}_r &= \dot{q}_d - \lambda_p e = Q_\phi \dot{q}_d - \lambda_p e \\ e_v &= \dot{q} - \dot{q}_r \\ e_{vn} &= P_\phi e_v \end{aligned}$$

where λ_p is a positive gain. Substituting the control law into the dynamic equations, we obtain the error dynamics

$$M(q) \dot{e}_v + C(q, \dot{q}) e_v + F_v e_v = -\lambda_{tn} P_\phi \text{sgn}(e_{vn}). \quad (19)$$

1) *Stability*: Consider the following Lyapunov function candidate:

$$V(q, e_v) = \frac{1}{2} e_v^T M(q) e_v. \quad (20)$$

Taking the derivative of the Lyapunov function candidate along the trajectories of (19), using the skew-symmetry of the matrix $\dot{M} - 2C$, and simplifying, we obtain

$$\dot{V}(e_v) = -e_v^T F_v e_v - \lambda_{tn} e_v^T P_\phi \text{sgn}(e_{vn}). \quad (21)$$

Since $e_{vn} = P_\phi e_v$ and $P_\phi^T = P_\phi$, the derivative of the Lyapunov function candidate can be bounded as follows:

$$\dot{V}(e_v) \leq -\sigma_v \|e_v\|^2 - \lambda_{tn} |e_{vn}|. \quad (22)$$

Therefore, (20) and (22) mean that $V(e_v)$ is, indeed, a Lyapunov function, i.e., V is positive definite and its time derivative along the trajectories of (19) is negative definite. Hence, e_v converges to zero asymptotically. Further, since $e_v = P_\phi e_v + Q_\phi e_v$, projection of e_v in both tangential and normal directions is zero. Thus, e_{vn} converges to zero asymptotically.

In the preceding, we have shown that the Lyapunov function decreases between impacts. If a series of impacts are involved during the transition phase, decrease of the Lyapunov function after every impact needs to be shown. The impact model given by (9) describes the behavior of the robot at the moment of impact with the constraint surface. Let A^- and A^+ represent a variable or function before and after an impact. Assume that the robot end-effector impacts the constraint surface at time instants t_k , where $k = 0, 1, 2, \dots$ is the number of impact points. Let $e_{vk}^+ = e_v(t_k + \delta)$ and $e_{vk}^- = e_v(t_k - \delta)$, where $\delta \rightarrow 0$. The Lyapunov function change during the k th impact can be simplified as follows:

$$\begin{aligned} \Delta V_k &:= V_k^+ - V_k^- \\ &= \frac{1}{2} (e_{vk}^+)^T M(q) (e_{vk}^+) - \frac{1}{2} (e_{vk}^-)^T M(q) (e_{vk}^-) \\ &= \frac{1}{2} (\dot{q}_k^+ - \dot{q}_{kr})^T M(q) (\dot{q}_k^+ - \dot{q}_{kr}) \\ &\quad - \frac{1}{2} (\dot{q}_k^- - \dot{q}_{kr})^T M(q) (\dot{q}_k^- - \dot{q}_{kr}) \\ &= \frac{1}{2} (\dot{q}_k^+)^T M(q) (\dot{q}_k^+) - \frac{1}{2} (\dot{q}_k^-)^T M(q) (\dot{q}_k^-) \\ &\quad - [(\dot{q}_{kr})^T M(q) (\dot{q}_k^+) - (\dot{q}_{kr})^T M(q) (\dot{q}_k^-)] \\ &= \mathcal{K}_k^+ - \mathcal{K}_k^- - (\dot{q}_{kr})^T M(q) (\dot{q}_k^+ - \dot{q}_k^-) \\ &= -\Delta \mathcal{K}_k - (\dot{q}_{kr})^T M(q) \Delta \dot{q}_k. \end{aligned}$$

Using (12) and noting that $\dot{q}_{kr} = Q_\phi (\dot{q}_{kd} - \lambda_p e_k)$, we obtain

$$\begin{aligned} \Delta V_k &= -\Delta \mathcal{K}_k - (\dot{q}_{kd} - \lambda_p e_k)^T F_I \\ &= -\Delta \mathcal{K}_k - (\dot{q}_{kd} - \lambda_p e_k)^T Q_\phi^T F_I. \end{aligned}$$

Since $Q_\phi^T F_I = 0$, we obtain

$$V_k^+ - V_k^- = -\Delta \mathcal{K}_k \leq 0. \quad (23)$$

Therefore, the Lyapunov function is decreasing during impact.

C. Motion and Force Control During Constrained Motion Phase

The constrained motion phase starts when the robot end-effector is in stable contact with the constraint surface. During this phase, manipulator dynamics are

$$M(q) \ddot{q} + C(q, \dot{q}) \dot{q} + g(q) = \tau + v(q) f_n. \quad (24)$$

For this phase, we choose the following control law given in [1]:

$$\tau = M(q)\ddot{q}_r + C(q, \dot{q})\dot{q}_r + g(q) - F_v e_v - v(q)(f_{nd} - \eta e_{vfn}) \quad (25)$$

where f_{nd} is the desired normal force, η is a positive gain, and

$$\begin{aligned} \dot{q}_r &= Q_\phi[\dot{q}_d - \Lambda_p e] + \beta_f \bar{v}(q) e_{vfn} \\ \ddot{q}_r &= Q_\phi[\ddot{q}_d - \Lambda_p \dot{e}] + \dot{Q}_\phi[\dot{q}_d - \Lambda_p e] \\ &\quad + \beta_f \bar{v}(q) e_{fn} + \beta_f \dot{\bar{v}}(q) e_{vfn} \\ e_v &= \dot{q} - \dot{q}_r \\ \bar{v}(q) &= v(q)/\|v(q)\|^2 \\ e_{fn} &= f_n - f_{nd} \\ e_{vfn} &= \int_0^t e_{fn}(\omega) d\omega. \end{aligned}$$

Substituting the control law (25) into the dynamic equation (24), we obtain

$$M(q)\dot{e}_v + C(q, \dot{q})e_v + F_v e_v = v(q)(e_{fn} + \eta e_{vfn}). \quad (26)$$

Stability analysis of the closed-loop dynamics can be found in [1].

D. Controller for a Complete Task

The controller for a complete task is composed of controllers from each phase based on a control-switching strategy. An event-based control switching strategy is developed for the complete task. In the free motion phase, a model-based adaptive control law is applied for trajectory tracking considering robot model uncertainties. Upon contact with the surface, control is switched to the one given by (18). In the transition phase, the primary goal is to stabilize the robot end-effector onto the surface. When the end-effector is on the surface, we switch to the constrained motion control law given by (25). Event-based online trajectory planning is utilized along with the control switch strategy. The desired trajectory is precomputed based on the initial knowledge of the location of the constraint surface. Immediately after the first impact, precomputed trajectories are modified such that the desired velocity normal to the constraint surface is zero. After the completion of the transition phase, the trajectory planner prescribes a desired force in the direction normal to the constraint surface and a desired joint space trajectory projected into the tangential direction of the constraint surface. Notice that the reference velocity e_v in each phase is different even though we use the same notation. So, comparison of Lyapunov function between phases is not practical. The closed-loop system is shown to be stable in each phase, and the robot system states are bounded when switching from one phase to the another. Hence, a stability concept similar to the one given by [23, Lemma 8.3] can be used for the proposed framework.

IV. EXPERIMENTS

A. Experimental Platform

The platform for robotic surface following experiments consists of a two-link robot system, a computer for real-time control, and a constraint fixture, as shown in Fig. 1. The main part of the robot system is a two-axis direct drive manipulator, as

shown in Fig. 1. Each axis is driven by an NSK-Megatorque direct drive servo-motor, which is capable of up to three revolutions per second maximum velocity and position feedback resolution of up to 156 400 counts per revolution. The base motor delivers up to 245 Nm of torque output, and the elbow motor delivers up to 40 Nm of torque output. The length of manipulator link 1 and link 2 are 0.36 and 0.24 m, respectively.

The dynamics of the two-link manipulator are given by

$$M(q)\ddot{q} + C(q, \dot{q})\dot{q} = \tau \quad (27)$$

where $M(q)$ is the mass matrix and $C(q, \dot{q})$ is the matrix composed of Coriolis and centrifugal terms. These two matrices are linear in terms of the coupled manipulator inertial parameters. Hence, the left-hand side of (27) can be written as

$$M(q)\ddot{q} + C(q, \dot{q})\dot{q} = Y(q, \dot{q}, \ddot{q})\beta$$

where $\beta = [p_1, p_2, p_3]^T$ is the manipulator parameter vector and $Y(q, \dot{q}, \ddot{q})$ is the regressor matrix given by

$$Y = \begin{bmatrix} \ddot{q}_1 & \ddot{q}_2 & c_2(2\ddot{q}_1 + \ddot{q}_2) - s_2\dot{q}_2(2\dot{q}_1 + \dot{q}_2) \\ 0 & \ddot{q}_1 + \ddot{q}_2 & \ddot{q}_1 c_2 + \dot{q}_1^2 s_2 \end{bmatrix}$$

where $c_2 = \cos(q_2)$ and $s_2 = \sin(q_2)$.

A six-axes force sensor is mounted on the end of the second-link of the robot manipulator. The force sensor has an on-board digital signal processor (DSP), which can provide force sensor data up to a sampling frequency of 3 kHz. Provision is also available for tool weight offset, filtering, temperature compensation, and coordinate frame rotation. The computer system consists of a computer workstation, the direct drive manipulator controller, and I/O cards associated with the sensors. The direct drive manipulator controller is used for real-time control and data acquisition. The controller is a three-processor system consisting of a host Pentium processor, a servo DSP, and a force sensor DSP. The end-effector, which is a circular metal disk holding a cylindrical metal tip via a smooth ball bearing, is attached to the force sensor. The metal tip follows the constraint surface along a desired trajectory while applying a desired normal force.

B. Constraint Surface and Desired Trajectory

The constraint surface is chosen as a rigid straight wall, which is a thick aluminum sheet firmly held by a vice as shown in Fig. 2. Fig. 3 illustrates the two-link robot (top view) and the constraint surface in the Cartesian space. In Fig. 3, the desired trajectory of the robot is **CDABC** (bold line). The uncertainty in the constraint location is represented by ζ . Therefore, depending on the uncertainty there are the following three possibilities:

- 1) $\zeta = 0$: there is no normal velocity at contact, i.e., the robot lands on the surface smoothly;
- 2) $\zeta > 0$: the robot end-effector will impact the surface with nonzero normal velocity anywhere along the path **DA**;
- 3) $\zeta < 0$: the robot will not make contact with the surface.

When case 3) is encountered, the proposed control algorithm simply performs motion control along the desired trajectory. We show experimental results of cases 1) and 2) with the proposed

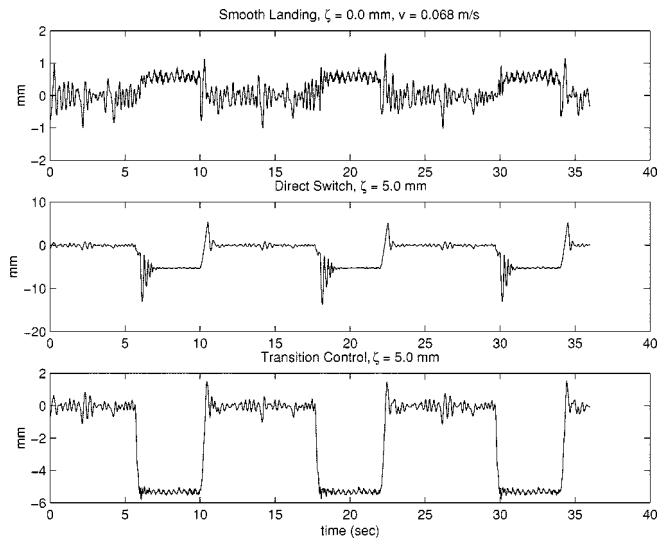


Fig. 4. Normal position error, low speed.

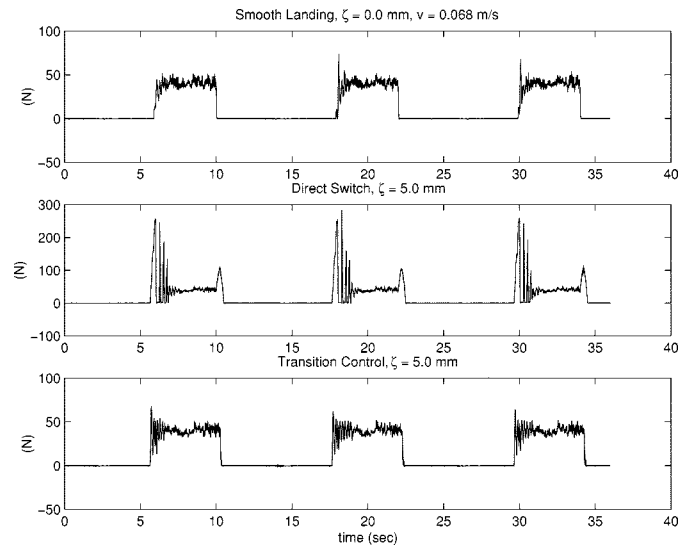


Fig. 6. Normal force, low speed.

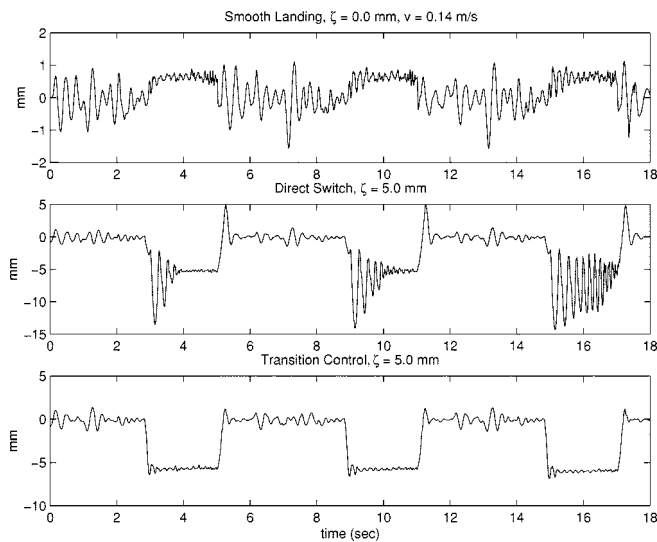


Fig. 5. Normal position error, high speed.

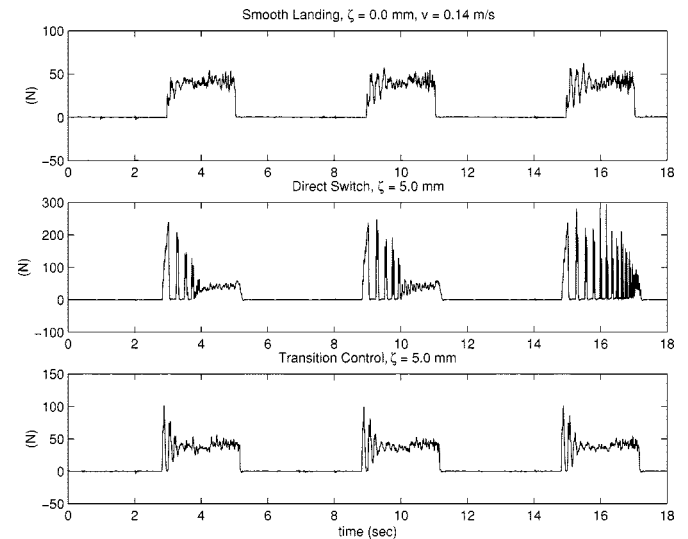


Fig. 7. Normal force, high speed.

trajectory sections **CD**, **DA**, and **BC**. Constrained motion and force control is applied along the surface **AB**. Transition control is activated at the first impact. In the direct switch algorithm, constrained motion and force control is activated according to the design of the precomputed desired trajectory, i.e., at point **A**, ignoring transition. In all the experiments, a servo sampling rate of 250 Hz is employed. Since force measurements are very noisy, a fixed-length moving average filter is used to filter noisy force measurements. Also, since the force data can be collected at higher sampling rates, a force sensor sampling rate of 2 kHz is used. The higher force sampling rate reduces delay introduced due to filtering.

The results for each experiment, shown in Figs. 4–15, correspond to consecutive implementation of three cycles of the desired trajectory. Fig. 4 shows the normal position error for low speed ($v = 0.068$ m/s) for three cases: 1) smooth landing (no uncertainty, $\zeta = 0$ mm), 2) direct switch ($\zeta = 5$ mm), and 3) transition control ($\zeta = 5$ mm). Fig. 5 gives experimental results for high speed ($v = 0.14$ m/s). The desired normal force

is 45 N. Notice that if we do not apply any transition control at impact, the robot bounces severely on the constraint surface. When we apply the transition controller, the robot settles on the surface after the first bounce. For the direct switch case, it should be observed that the end-effector tip seems to go into the surface, which is due to the compliance of the end-effector assembly and/or surface. Figs. 6 and 7 give the normal force for low and high speeds, respectively, for the three cases. The results show that directly switching from free motion control to constrained motion and force control results in severe bounces of the robot on the surface. This effect is magnified for the high speed case. Figs. 8 and 9 give the tangential force for low and high speeds, respectively. The tangential force data shows that the surface has some friction. To better illustrate the bounces on the surface, Cartesian trajectories are plotted in Figs. 10 and 11. In these figures, the dashed line represents the actual location of the constraint surface. The dotted line represents the precomputed desired trajectory of the robot tip, which is based on the

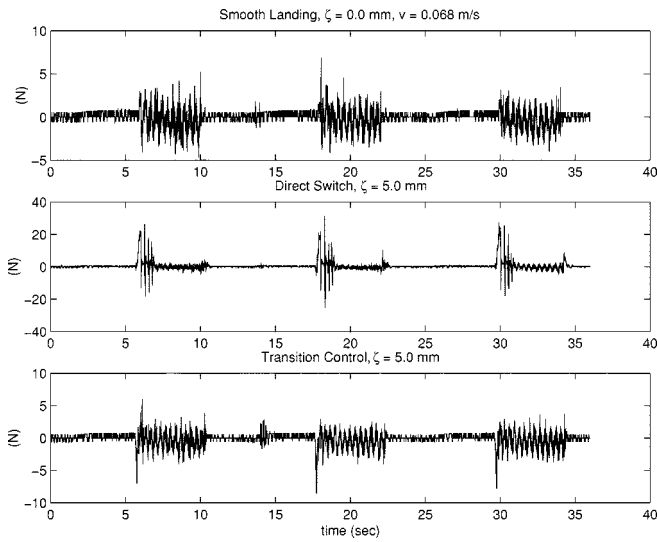


Fig. 8. Tangential force, low speed.

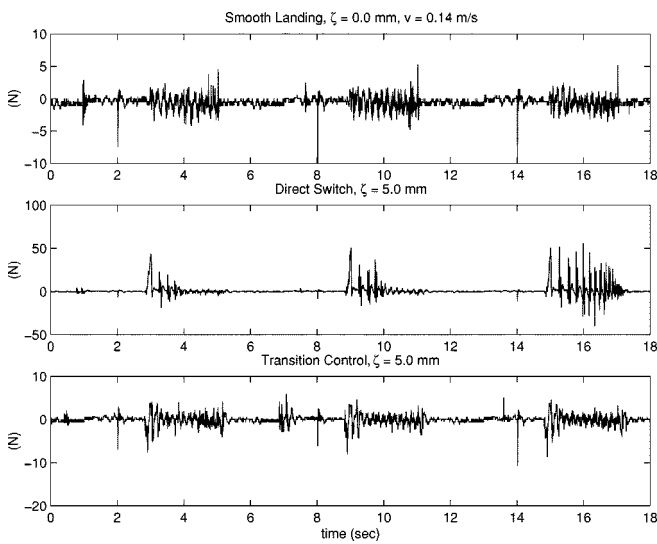


Fig. 9. Tangential force, high speed.

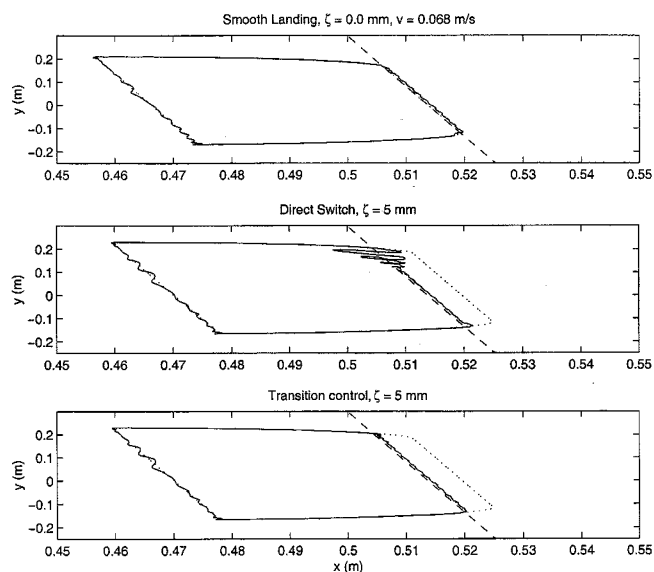


Fig. 10. Cartesian trajectory, low speed.

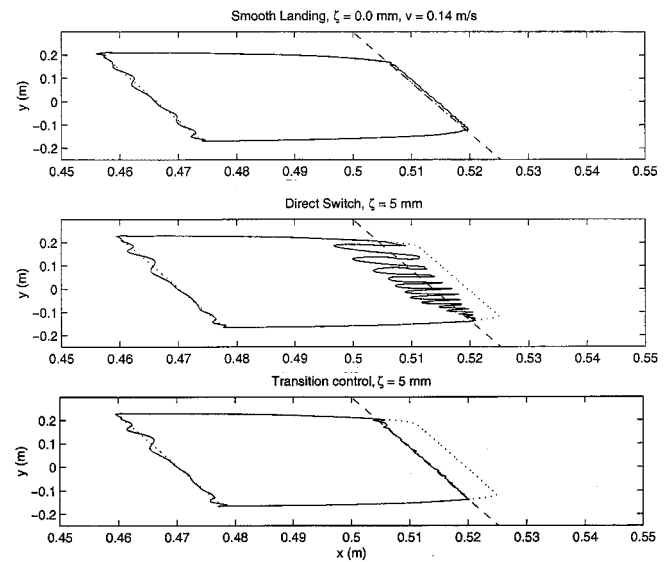
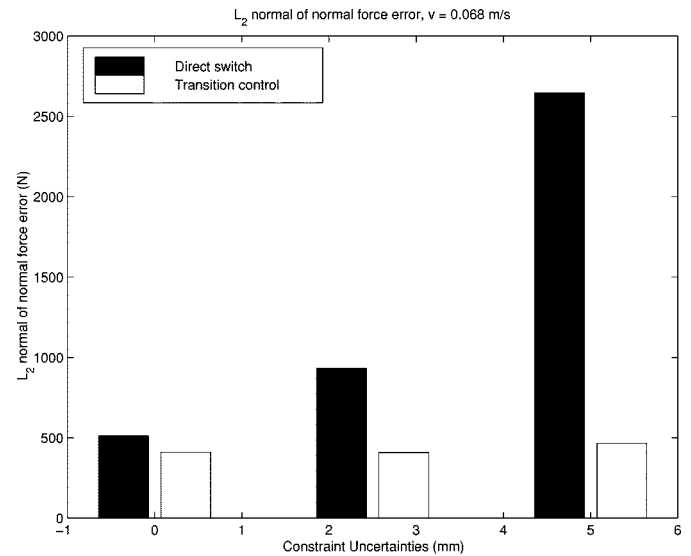


Fig. 11. Cartesian trajectory, high speed.

Fig. 12. Normal force error L_2 norm, low speed.

a priori knowledge of the location of the constraint. The solid line is the actual path followed by the robot tip.

Figs. 12 and 13 give the L_2 norm of the normal force error for direct switch and transition control. With no constraint uncertainty, $\zeta = 0.0$ mm, both direct switch and transition control give similar performance, as expected. With constraint uncertainties $\zeta = 2.5$ and 5.0 mm, the performance is much better with the transition controller.

Further, to illustrate the performance of the proposed control algorithm, we show experimental results when the uncertainty is 7.5 mm in Figs. 14–16. To focus on the behavior of the robot tip in the transition phase, Fig. 16 shows the Cartesian trajectory and the normal force for a short duration of time around the transition phase. The first impact with the constraint surface is denoted by “ \ast ” in Fig. 16. Notice that the normal force becomes zero after a short duration of time after the first impact, which means that at point 1, the robot leaves the constraint surface. Also, from the Cartesian trajectory, it appears that at

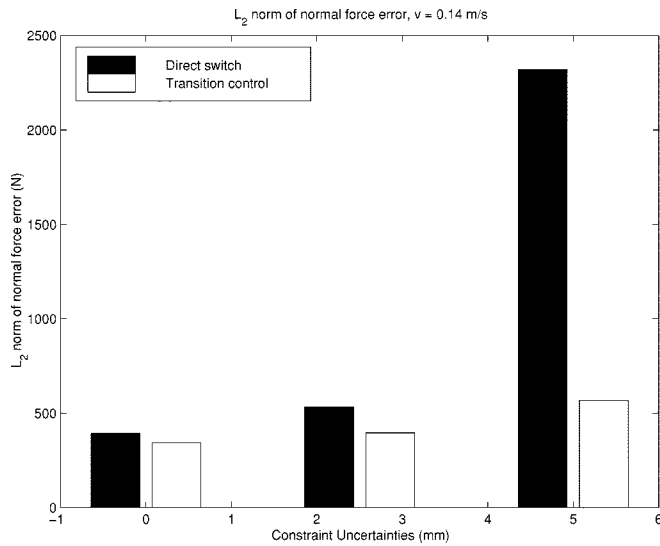


Fig. 13. Normal force error L_2 norm, high speed.

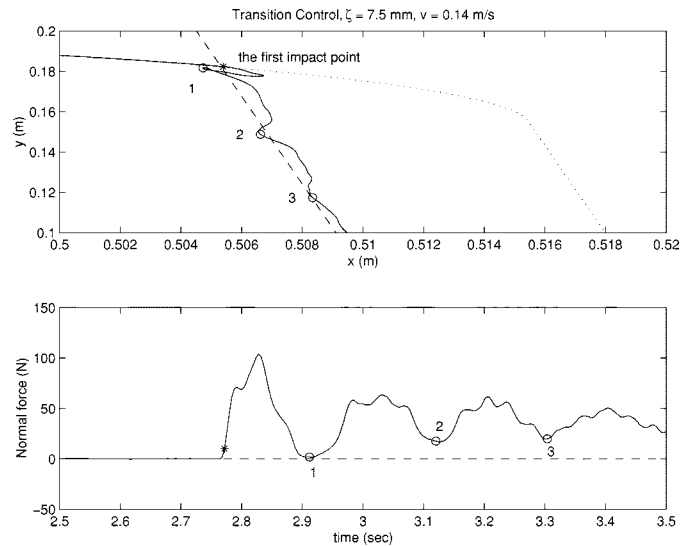


Fig. 16. Motion and force near impact, transition control, $\zeta = 7.5$ mm.

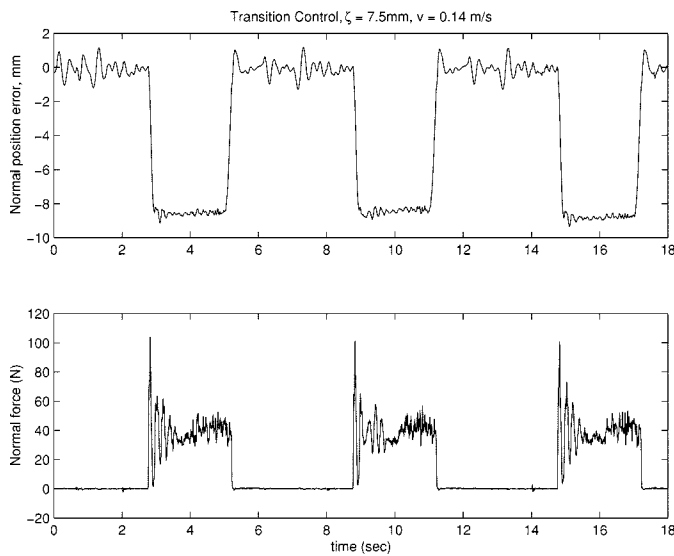


Fig. 14. Normal error and normal force using transition control, $\zeta = 7.5$ mm.

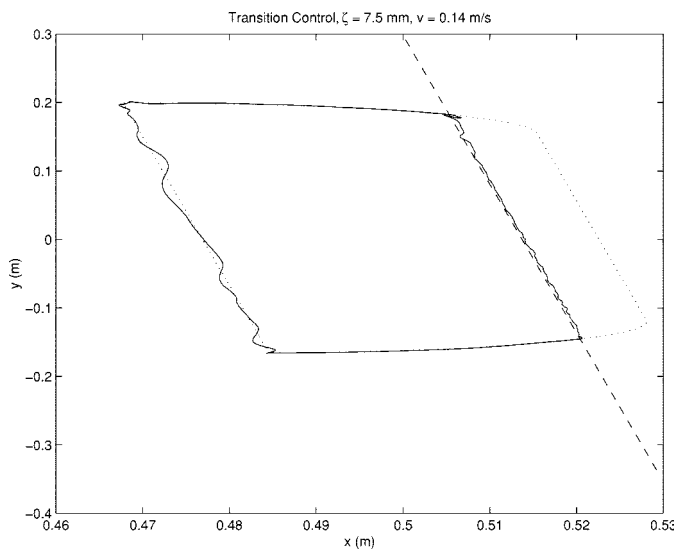


Fig. 15. Cartesian trajectory using transition control, $\zeta = 7.5$ mm.

TABLE I
SUMMARY: PEAK NORMAL FORCE (N)

	$v = 0.14$ m/s		$v = 0.068$ m/s	
	DS	TC	DS	TC
0.0 mm	62.3	56.1	73.7	56.4
2.5 mm	101.5	63.5	136.9	52.4
5.0 mm	293.8	101.3	282.8	67.9
7.5 mm	No data	104.0	No data	65.5

TABLE II
SUMMARY: NUMBER OF REBOUNDS

	$v = 0.14$ m/s		$v = 0.068$ m/s	
	DS	TC	DS	TC
0.0 mm	0	0	0	0
2.5 mm	2	0	2-3	0
5.0 mm	4-15	1	4	0
7.5 mm	No data	1	No data	0

points 2 and 3 the robot tip leaves the surface. But this is not the case, since the normal force magnitude at points 2 and 3 is nonzero. Although the surface is rigidly fixed to the vice, there is some compliance in the surface and the end-effector assembly that causes small vibrations after the impact. Therefore, with the proposed transition controller, even for a constraint uncertainty of 7.5 mm we can observe stable landing of the robot tip on the surface with just one bounce. For this level of uncertainty, the direct switch algorithm renders the system unstable.

In addition to the given figures, we summarize the results of numerous experiments in Tables I and II. Table I gives a summary of the peak normal force and Table II gives the number of bounces of the robot tip on the constraint surface. The notation used in the tables are as follows. **CU**: constraint uncertainty; **DS**: direct switch; and **TC**: transition control. Experimental data summarized in Tables I and II show that the impact force peaks and the number of bounces are reduced when we apply transition control. The effectiveness of the transition controller and

the entire control strategy is confirmed by these experimental results.

V. CONCLUSION

In this paper, we proposed a new stable control algorithm for transition from free motion to constrained motion for robots. Uncertainty in the location of the constraint surface will cause impact of the robot with the surface. Control of transition from free motion to constrained motion is essential to maintain stability of the system when the constraint location is uncertain. A stable discontinuous controller is proposed for the transition phase. Extensive experiments were conducted for a complete robot task with different levels of constraint uncertainty and travel velocities on the surface. Experimental results validate the effectiveness of the proposed control strategy. Future research will focus on actual robotic surface finishing experiments using the proposed control strategy. Also, the proposed control design does not consider any uncertainty in the orientation of the constraint. An uncertainty in the orientation would mean that the gradient of the constraint surface is uncertain, and thus the projection matrices will be uncertain. This will be a topic of future research. In the future, we also plan to investigate the effects of surface compliance and friction.

REFERENCES

- [1] S. Arimoto, *Control Theory of Non-Linear Mechanical Systems—A Passivity-Based and Circuit-Theoretic Approach*. New York: Oxford Univ. Press, 1996.
- [2] J.-J. E. Slotine and W. Li, *Applied Nonlinear Control*. Englewood Cliffs, NJ: Prentice-Hall, 1991.
- [3] T. Yoshikawa, "Dynamic hybrid position-force control of robot manipulators—Description of hand constraint and calculation of joint driving force," *IEEE Trans. Robot. Automat.*, vol. RA-3, pp. 386–392, 1987.
- [4] M. Raibert and J. Craig, "Hybrid position/force control of manipulator," *ASME J. Dyn. Syst., Meas. Contr.*, vol. 102, pp. 126–133, 1988.
- [5] D. Wang and N. H. McClamroch, "Position and force control for constrained manipulator motion: Lyapunov's direct method," *IEEE Trans. Robot. Automat.*, vol. 9, pp. 308–312, June 1993.
- [6] R. Volpe and P. Kholsa, "A theoretical and experimental investigation of explicit force control strategies for manipulators," *IEEE Trans. Automat. Contr.*, vol. 38, pp. 1734–1650, Nov. 1993.
- [7] L. L. Whitcomb and S. Arimoto, "Adaptive model-based hybrid control of geometrically constrained robot arms," *IEEE Trans. Robot. Automat.*, vol. 13, pp. 105–116, Feb. 1997.
- [8] Y. F. Zheng and H. Hemami, "Mathematical modeling of a robot collision with its environment," *J. Robot. Res.*, vol. 13, pp. 289–307, 1985.
- [9] N. Hogan, "Impedance control: An approach to manipulation: Part I—Theory; part II—Implementation; part III—Applications," *ASME J. Dyn. Syst., Meas. Contr.*, vol. 107, pp. 1–24, 1985.
- [10] H. Kazerooni, T. Sheridan, and P. Houpt, "Robust compliant motion for manipulators," *IEEE Trans. Robot. Automat.*, vol. RA-2, pp. 83–105, Apr. 1986.
- [11] G. Niemeyer and J. J. E. Slotine, "Computational algorithms for adaptive compliant motion," in *Proc. IEEE Int. Conf. Robotics and Automation*, 1989, pp. 566–571.
- [12] J. K. Mills and D. M. Lokhorst, "Stability and control of robotic manipulators during contact/noncontact task transition," *IEEE Trans. Robot. Automat.*, vol. 9, pp. 335–346, June 1993.

- [13] P. R. Pagilla and B. Yu, "Design and experimental evaluation of a stable transition controller for geometrically constrained robots," in *Proc. IEEE Int. Conf. Robotics and Automation*, San Francisco, CA, 2000.
- [14] P. R. Pagilla and M. Tomizuka, "Contact transition control of nonlinear mechanical systems subject to a unilateral constraint," *ASME J. Dyn. Syst., Meas. Contr.*, vol. 119, pp. 749–759, 1997.
- [15] T. J. Tarn, Y. Wu, N. Xi, and A. Isidori, "Force regulation and contact transition control," *IEEE Contr. Syst. Mag.*, pp. 32–40, Feb. 1996.
- [16] K. Youcef-Toumi and D. A. Gutz, "Impact and force control: Modeling and experiments," *ASME J. Dyn. Syst., Meas. Contr.*, vol. 116, no. 1, pp. 89–98, 1994.
- [17] A. A. ten Dam, E. Dwarshuis, and J. C. Willems, "The contact problem for linear continuous time dynamical systems: A geometric approach," *IEEE Trans. Automat. Contr.*, vol. 42, pp. 458–472, Apr. 1997.
- [18] B. Brogliato, S. Niclescu, and P. Orhant, "On the control of finite dimensional mechanical systems with unilateral constraints," *IEEE Trans. Automat. Contr.*, vol. 42, no. 2, pp. 200–215, Feb. 1997.
- [19] A. Tornambe, "Modeling and control of the impact in mechanical systems: Theory and experimental results," *IEEE Trans. Automat. Contr.*, vol. 44, pp. 294–309, Feb. 1999.
- [20] W. Goldsmith, *Impact: The Theory and Physical Behavior of Colliding Solids*. London, U.K.: E. Arnold, 1960.
- [21] R. M. Brach, *Mechanical Impact Dynamics: Rigid Body Collisions*. New York: Wiley, 1991.
- [22] V. V. Kozlov and D. V. Treschev, "Billiards: A genetic introduction to the dynamics of systems with impacts," *Translations of Mathematical Monographs*, 1991.
- [23] B. Brogliato, *Nonsmooth Impact Mechanics: Models, Dynamics, and Control*, London, U.K.: Springer-Verlag, 1996.
- [24] J. B. Keller, "Impact with friction," *ASME J. Appl. Mech.*, vol. 53, pp. 1–4, 1985.
- [25] C. E. Smith, "Predicting rebounds using rigid body dynamics," *ASME J. Appl. Mech.*, vol. 58, pp. 754–758, 1991.
- [26] A. J. van der Schaft and J. M. Schumacher, "Complimentarity modeling of hybrid systems," *IEEE Trans. Automat. Contr.*, vol. 43, pp. 483–490, Apr. 1998.
- [27] A. J. van der Schaft and H. Schumacher, *An Introduction to Hybrid Dynamical Systems*. New York: Springer-Verlag, 2000.



Prabhakar R. Pagilla (S'92–M'96) received the B.Eng. degree from Osmania University, Hyderabad, India, in 1990 and the M.S. and Ph.D. degrees from the University of California, Berkeley, in 1994 and 1996, respectively, all in mechanical engineering.

He is currently an Assistant Professor in the School of Mechanical and Aerospace Engineering, Oklahoma State University, Stillwater. His research activities are mainly in the areas of nonlinear systems, adaptive control, constrained mechanical systems, large-scale systems, mechatronics, and

Web-handling processes.

Dr. Pagilla received a National Science Foundation CAREER Award in 2000.



Biao Yu received the B.S. degree in manufacturing engineering from Beijing University of Aeronautics and Astronautics, Beijing, China, in 1990 and the M.S. degree in mechanical engineering from South China University of Technology, Guangzhou, China, in 1993. He is currently working toward the Ph.D. degree in the School of Mechanical and Aerospace Engineering, Oklahoma State University, Stillwater.

His current research interests lie in adaptive control, mechatronics, real-time systems, and microprocessor-based systems.